Journal of Power Sources 261 (2014) 28–37

Contents lists available at ScienceDirect

Journal of Power Sources

journal homepage: www.elsevier.com/locate/jpowsour

Measurements of heat generation in prismatic Li-ion batteries

Kaiwei Chen, Grant Unsworth, Xianguo Li*

20/20 Laboratory for Fuel Cell and Green Energy RD&D, Department of Mechanical and Mechatronics Engineering, University of Waterloo, Waterloo, ON N2L 3G1 Canada

HIGHLIGHTS

- Developed a calorimeter for heat generation measurement of prismatic batteries.
- Measured battery heat generation from −10 °C to 40 °C and 0.25C–3C discharge rates.
- Observed endothermic heat flow at low discharge rates and 30 °C–40 °C temperatures.
- Observed non-negligible heat of mixing at discharge rates as low as 0.25C.
- Observed a double plateau in battery discharge curve for 30 °C–40 °C temperatures.

ARTICLE INFO

Article history:
Received 8 November 2013
Received in revised form
3 March 2014
Accepted 11 March 2014
Available online 20 March 2014

Keywords:
Lithium-ion battery
Heat generation
Experimental measurement
Calorimetry

ABSTRACT

An accurate understanding of the characteristics of battery heat generation is essential to the development and success of thermal management systems for electric vehicles. In this study, a calorimeter capable of measuring the heat generation rates of a prismatic battery is developed and verified by using a controllable electric heater. The heat generation rates of a prismatic A123 $LiFePO_4$ battery is measured for discharge rates ranging from 0.25C to 3C and operating temperature ranging from −10 °C to 40 °C. At low rates of discharge the heat generation is not significant, even becoming endothermic at the battery operating temperatures of 30 °C and 40 °C. Heat of mixing is observed to be a non-negligible component of total heat generation at discharge rates as low as 0.25C for all tested battery operating temperatures. A double plateau in battery discharge curve is observed for operating temperatures of 30 °C and 40 °C. The developed experimental facility can be used for the characterization of heat generation for any prismatic battery, regardless of chemistries.

1. Introduction

Rechargeable Lithium ion (Li-ion) batteries are commonly used as an energy storage medium for electric and hybrid electric vehicles (EVs and HEVs) due to their superior power density (>240 Wh kg^{-1}) and non-existent memory effects [1–3]. However, low temperature performance and high temperature capacity degradation are major limitations of the technology [4–7]. Batteries need to be maintained within an optimal temperature range to minimize degradation and avoid thermal runaway [8], irregardless of the ambient temperature that the EV or HEV is operating in. The design of a thermal management system capable of this requires knowledge of Li-ion battery heat generation rates over a wide range of operating temperatures and discharge conditions.

Heat generation in Li-ion batteries includes two main components: reversible heat generation due to entropic changes in the battery, and irreversible heat generation due to ohmic losses, charge-transfer overpotentials, and mass transfer limitations [9]. High current densities at the current collectors also create additional Joule heating, particularly in large form batteries such as the prismatic type used in EVs and HEVs [10–13]. These forms of heat generation are temperature dependent and, due to the complexity of the system, must be measured experimentally for specific batteries.

Heat generation rates of Li-ion batteries have been measured using two methods: accelerated-rate calorimetry (ARC) and iso thermal heat conduction calorimetry (IHC).

The ARC method determines the heat generation rate of the battery by measuring the rise in battery temperature over time and the amount of heat expelled from the battery to the

* Corresponding author.
E-mail address: xianguo.li@uwaterloo.ca (X. Li).

http://dx.doi.org/10.1016/j.jpowsour.2014.03.037
0378-7753/

surroundings. Li-ion batteries have a layered internal structure, and hence it is difficult to measure its heat capacity accurately. Since the battery is an electrochemical device, changes in the battery temperature during testing could lead to inaccurate heat generation characterization [15]. Hong et al. used a commercially available accelerated rate calorimeter (ARC2000, Columbia Scientific Industries) to measure the heat generation rates of Sony type US18650 1.35 Ah cylindrical Li-ion battery at discharge rates of 0.33C, 0.5C, and 1C at 308 K, with the maximum measured heat generation rates of 1.63 WL^{-1} [16]. Al Hallaj et al. made measurements with the same experimental apparatus on 18650 Li-ion batteries from AT&T and Panasonic, and found maximum heat generation rates of 0.26 WL^{-1} for discharge rates of less than 0.1C and charge rates of 0.33C [17].

The IHC method utilizes a large heat sink in contact with the surface of the battery to keep the battery at isothermal operation during measurements. This technique confines the measurements to low battery discharge rates, since fast discharge of the battery leads to higher rates of heat generation which the heat sink cannot extract, causing a temperature gradient within the battery [1]. Kim et al. utilized a commercially available micro-calorimeter (IMC, CSC4400, Calorimetry Science Corp.) to classify the heat generation rates of Li-ion coin type (size 2016) batteries. The heat generation rate of the battery was measured using temperature sensors placed between the battery and an aluminium heat sink and for discharge rates of 0.1C, 0.2C, 0.33C, and 1C from 300 K to 330 K. The corresponding maximum heat generation rates were reported as 0.82 WL^{-1} for discharge rates between 0.1C and 0.2C, 0.97 WL^{-1} for discharge rates of 0.2C–0.5C, and 3.21 WL^{-1} for discharge rates of 0.5C–1C [18]. Kobayashi et al. measured the heat generation rates of cylindrical Sony US18650 Li-ion batteries using a Calvet-type conduction micro-calorimeter (MMC5111-U), which has an isothermal aluminium vessel in contact with the test battery, and a thermomodule was used to measure the amount of heat transfer from the battery to the heat sink. The battery was discharged at 1/50C and 1/10C at an ambient temperature of 300 K and 330 K, and a maximum heat generation rate of 0.97 WL^{-1} was measured for discharge rates between 0.1C and 0.2C [19]. Onda et al. measured the heat generation rates of small cylindrical Sony US18650 Li-ion batteries using a thermal bath as the constant temperature heat sink. The test battery was wrapped in a thin film for electrical insulation, and the temperature of the battery was recorded using a type K thermocouple. The battery was discharged at 0.1C, 0.5C, and 1C, with a corresponding maximum measured heat generation rate of 11.0 WL^{-1}, 27.5 WL^{-1} m and 84.5 WL^{-1} [20]. Bang et al. used the same equipment as Kim et al. to perform in situ heat generation rates of a $LiMn_2O_4$ coin type Li-ion cell. Measurements were performed at discharge rates of 0.1C, 0.14C, 0.33C, and 1C at battery temperatures between 300 K and 330 K. The results show a maximum heat generation rate of 0.63 WL^{-1} for discharge rates of 0.1C–0.2C, 2.65 WL^{-1} for discharge rates of 0.2C–0.5C, and 7.51 WL^{-1} for discharge rates of 0.5C–1C [21].

From the above literature review, it is clear that the previous works on the heat generation measurement of Li-ion batteries have exhibited a wide range of results, even for batteries of the same chemistry and form [1]; and they are limited to: (*i*) small sized cylindrical or coin type batteries which are not applicable for HEV and EV use; (*ii*) low rates of discharge ($\leq$1C) which are not representative of the electrical needs of the EV; (*iii*) battery operation near room temperatures, which do not reflect the wide range of operating temperatures of EVs. Therefore, the objective of the present study is to measure the heat generation rates for large prismatic type of Li-ion batteries for a wide range of discharge rates and operating temperatures, as encountered by EVs and HEVs. In this work, an experimental technique that can accurately measure the heat generation rates of prismatic Li-ion batteries is developed, and the heat generation rates of an A123 prismatic $LiFePO_4$ battery with a 20 Ah capacity for use in automotive applications is measured and verified for various discharge and operating conditions.

2. Experimental

2.1. Experimental setup

In the present study, the calorimeter is constructed by surrounding the battery with a material of known thermal properties (hereafter referred to as calorimeter material) such that a temperature profile within the material can be deduced for any battery heat generation rate. Prismatic batteries have a high surface area to thickness ratio, which promotes heat transfer from its front and back faces. Hence, the calorimeter is in the form of two identical slabs attached to the front and back faces of the test battery. The heat generated by the battery is conducted through the slabs into a constant temperature heat sink. Measured temperature change within the calorimeter material due to the heat generated by the battery can be used to infer the unknown heat generation rate of the battery. For the calorimeter design process, heat generated by the battery is estimated to be in the range of 10 W, and simulations are performed to estimate the temperature rise in the different calorimeter materials of various thickness due to the heat generation rate. High density polyethylene (HDPE) is selected as the calorimeter material due to its stable thermal properties at the planned test temperatures and its high temperature rise due to the estimated heat generation rate of the battery.

An exploded view of the calorimeter is shown in Fig. 1. The Li-ion battery is placed between two HDPE slabs, both of which are five times the thickness of the battery. A coating of thermal grease is applied to the surface of the battery to minimize contact resistance between the battery and HDPE surfaces. The HDPE slabs with the battery are placed between two aluminium slabs. This prevents deformation of the softer HDPE material during assembly to ensure good surface contact between the battery face and the HDPE. The calorimeter is bolted together in eight locations, tightened in a criss-cross pattern to ensure even tightening, and is immersed in a constant temperature bath (ThermoFisher A25B, accuracy of $\pm$0.1 °C). The working fluid within the thermal bath is a 50-50 mixture of water-ethylene glycol, which allows measurements at sub-zero temperatures. Two high accuracy thermocouples (with accuracy of $\pm$0.1 °C) are embedded 4 mm away from the battery contact surface vertically into the HDPE material (one in each slab), centred on the battery. The placement of the thermocouple at the centre of the battery minimizes the edge effects of heat transfer from the HDPE to the surroundings. Two additional thermocouples are placed at the surface of the battery to monitor the battery temperature throughout testing (not shown in Fig. 1). An insulating cover is placed over the assembly such that the battery terminals are exposed to air, which minimizes heat transfer from both the bath and the top of the calorimeter to the ambient. A schematic of the experimental apparatus is shown in Fig. 2.

The heat generation rate of a commercially available $LiFePO_4$ prismatic Li-ion battery from A123 with a nominal capacity of 20 Ah is measured, although any battery (Li-ion or otherwise) of prismatic shape can be used in the calorimeter. The battery measures 23 cm $\times$ 16 cm $\times$ 0.7 cm, and is controlled via Greenlight Innovations G12-200 multichannel battery test station, which has an accuracy of $\pm$0.2 A in current source control, $\pm$0.05 V in voltage

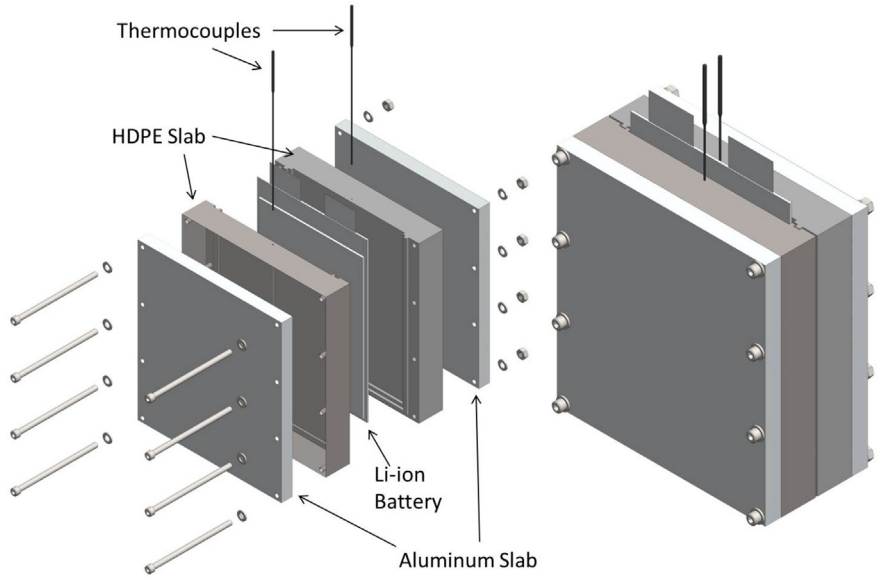

Fig. 1. Exploded (left) and assembled (right) view of the experimental setup for the measurement of heat generation of prismatic Li-ion batteries. HDPE denotes high density polyethylene.

source control, ±0.03 A in current sink control, and ±0.06 A in current measurement.

2.2. Experimental conditions and procedure

The discharge rates will be described in terms of C-rates, where 1C is the discharge rate at which the battery will be fully depleted in 1 h of operation (20 A for the test battery), 2C the rate at which the battery is fully depleted in 30 min (40 A), etc. The heat generation rates will be measured for five different battery discharge rates (0.25C, 0.5C, 1C, 2C, 3C), at six operating temperatures from −10 °C to 40 °C in 10 °C increments. The battery is cycled five times to the cut-off voltage of 2.6 V before testing, which allows irreversible capacity fade that may be present in unused Li-ion batteries to occur [16].

At the end of discharge, the battery is allowed to rest for 2 h before being charged back to the open circuit voltage of 3.6 V at a 0.2C charge rate under a constant voltage constant current charging

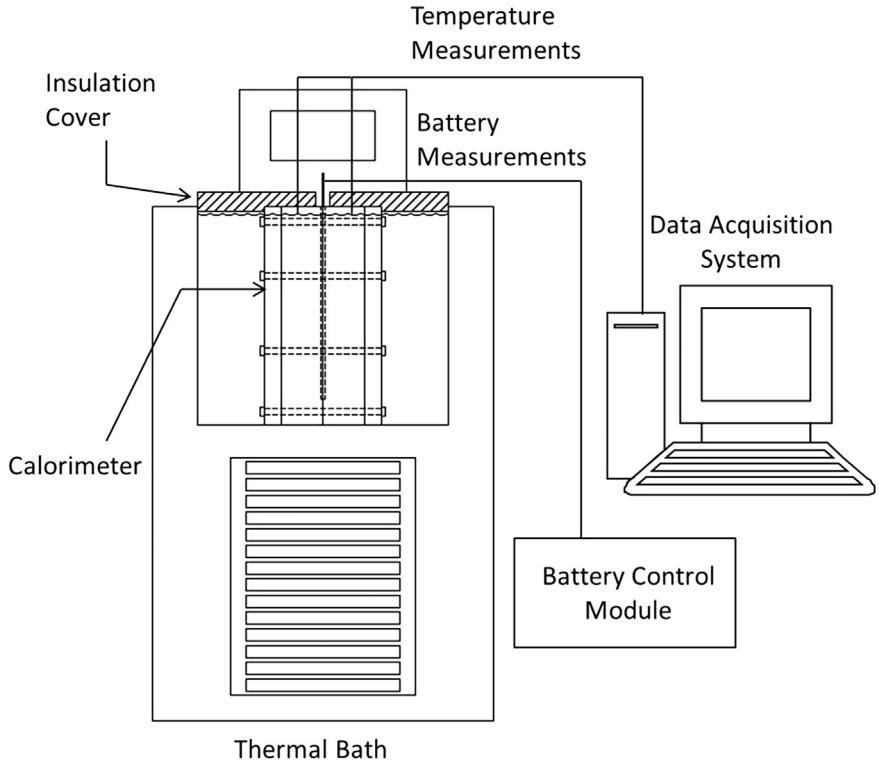

Fig. 2. Schematic of the experimental setup.

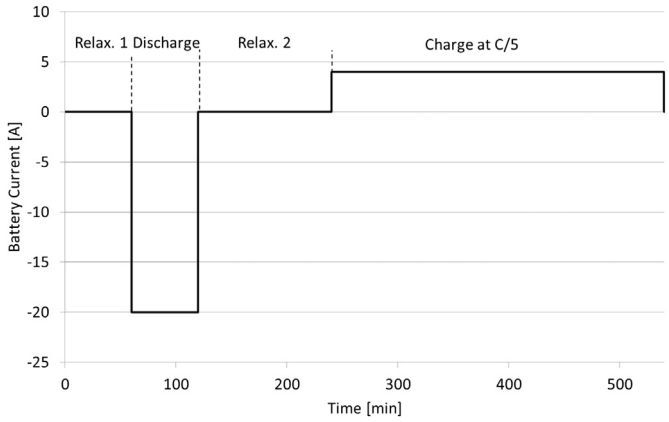

Fig. 3. Test schedule used in the present study for charging and discharging of the Li-ion battery.

scheme. Following the completion of charge, the battery is allowed to rest for an hour to ensure the equilibration of battery chemistry. The details of the charge and discharge schedule can be seen in Fig. 3.

2.3. Data reduction

A measured temperature change in the calorimeter allows the unknown heat generation rate of the battery to be inferred through the convolution theorem. The overall measured change in temperature, $\Delta T_m(t)$, of the calorimeter due to the battery's unknown heat generation, $\dot{q}(t)$, is defined as the sum of the responses of the system to a series of discrete pulses from t_o to t, which form a temporal discretization of the heat generation rate. This can be written as the integral [22],

$$\Delta T_m = \int_{t_o}^{t} \dot{q}(\tau)\phi(t-\tau)\mathrm{d}(\tau) \tag{1}$$

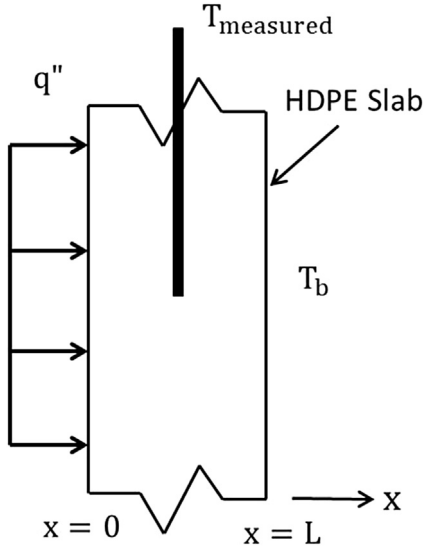

Fig. 4. Problem setup for the measurement of inner temperature of the high density polyethylene (HDPE) slab $T_{measured}$ from an imposed surface heat flux $\dot{q}''$ due to the heat generated in the test battery.

where $\phi(t-\tau)$ is the apparatus function, which is the response of the apparatus to a pulse heat generation. In this study, the apparatus function can be solved analytically using the heat diffusion equation and the material properties of HDPE according to the geometry in Fig. 4, which illustrates one-half of the calorimeter. The heat generated by the battery passing through the calorimeter is assumed to be one dimensional and the total heat generated by the battery, $\dot{q}$, is equal to two separate and equal heat fluxes, q''.

The measured temperature change at a specific location within the HDPE slabs due to the imposed heat flux ($\dot{q}''$) by the battery can be defined as $T_{measured}$. The temperature distribution within the HDPE slab is governed by Fick's law, and the following boundary and initial conditions

$$\begin{aligned} \frac{\partial^2 T}{\partial^2 x} &= \frac{1}{\alpha}\frac{\partial T}{\partial t} \\ T(x,0) &= T_b \\ T(L,t) &= T_b \\ -k\frac{\partial T}{\partial x}(0,t) &= q'' \end{aligned} \tag{2}$$

where α (2.46×10^{-7} m^2 s^{-1}) is the thermal diffusivity of the calorimeter material (HDPE in the present study), subscripts 0 and L denote the locations on the HDPE slabs at the contact with the battery and the aluminium slab respectively, and the subscript b denotes the temperature of the constant temperature bath, and k (0.53 Wm^{-1} K^{-1}) is the thermal conductivity of the calorimeter material. The temperature of the aluminium slabs can be assumed to be the same as the bath temperature due to its high thermal conductivity. The temperature increase at the measurement location x within the HDPE slab for a unit step increase in heat flux has to be found, such that

$$\Delta T_m = T_x(t) - T_b = q''[\phi(x,t)] \tag{3}$$

where $\phi(x,t)$ is the temperature rise at point x due to the applied heat flux. $\phi(x,t)$ can be found by solving the governing equations (Equations (2) and (3)), such that

$$T_x(t) - T_b = q''\left[\sum_{n=1}^{\infty}\frac{-1}{k}\left[\frac{8(-1)^{1+n}L}{\pi^2(4n^2-4n+1)}\right]\sin\left(\frac{(2n-1)\pi x}{2L}\right)\exp\left(-\left[\frac{(2n-1)\pi}{2L}\right]^2\alpha t\right)+\frac{x}{k}\right] \tag{4}$$

The convolution theorem can be applied using the apparatus function and the measured temperature change within the heat conduction medium. Owing to the discrete nature of the thermocouple measurements, $T_x(t)$, a discretized approximation of the convolution integral can be written as [23]

$$T_x(t) - T_b = \sum_{n=1}^{M} q_n''[\phi(x, t_{M-n+1}) - \phi(t_{M-n})] \tag{5}$$

Inverse heat conduction problems (IHCP) use a measured temperature change within a material of known thermal properties to infer a heat flux that is applied to one of the boundaries [23]. IHCPs are ill-posed, owing to the divergence of its solutions which may occur due to small perturbations in the measured temperature from either noise or random errors in the experiment [24,25]. For this study, Beck's Sequential Function Specification Method (Beck's Method) is used to introduce stability in the IHCP solution [23]. Beck's method increases the stability by introducing additional

information about the problem by specifying that the solution is temporally smooth. The method assumes that the unknown heat flux $\dot{q}''$ is temporarily fixed over a number of future time steps, r, with each time step having a period of Δt. Using Beck's Method, Equation (5) can be written in matrix form as [23]

$$\begin{pmatrix} \Delta\phi_0 & & & & & \\ \Delta\phi_1 & \Delta\phi_0 & & & & \\ \vdots & \vdots & \ddots & & & \\ \Delta\phi_{M-1} & \Delta\phi_{M-2} & \cdots & \Delta\phi_0 & & \\ \Delta\phi_M & \Delta\phi_{M-1} & \cdots & \Delta\phi_1 & \Delta\phi_0 & \\ \Delta\phi_{M+r-1} & \Delta\phi_{M+r-2} & \cdots & \cdots & \Delta\phi_1 & \Delta\phi_0 \end{pmatrix} \begin{pmatrix} q_1 \\ q_2 \\ \vdots \\ q_M \\ q_{M+1} \\ q_{M+r-1} \end{pmatrix} = \begin{pmatrix} T_1 \\ T_2 \\ \vdots \\ T_M \\ T_{M+1} \\ T_{M+r-1} \end{pmatrix} \tag{6}$$

The matrix of $\Delta\phi$'s represent the apparatus functions, which have been derived analytically from Equation (4). The matrix of T's represent the measured temperature change within the HDPE slabs due to the heat flux applied by the battery. The unknown heat flux at the surface of interest can be calculated using matrix manipulation techniques, after which it is then integrated to obtain the transient total heat generation rate of the battery. Exact solution to Equation (6) is obtained with an r value of 1, and the smoothness of the solution is increased with increasing values of r. An increase in r causes a decrease in sensitivity of the calculated heat flux at the surface of the HDPE slabs to oscillations in the temperature measurements, introducing more stability into the solution. Increased r values can also cause increased bias and decreased resolution in the calculated profile $\dot{q}''$, decreasing the values of the peaks in heat measurement. Therefore, the tuning parameters in Beck's Method needs to be carefully tuned to provide accurate results.

To tune the parameters in Becks method, Woodbury and Thackur defined a 'look ahead parameter', p, as [25]

$$p = r\Delta t \tag{7}$$

and showed that the calculated heat flux at the surface of interest has the same resolution and bias regardless of the value of r and Δt as long as p remains constant [25]. They concluded that adjustments need to be made to p such that the RMS error of the predicted temperature at any arbitrary location within the material is equivalent to the amount of noise in the measured data [25]. While manufacturer provided values for measurement errors can be used, Woodbury suggested experimentally determining the measurement errors to increase accuracy in ascertaining the value of p, which is the approach adopted in the presented study and will be described in the following section [25].

2.4. Calibration

Noise in the temperature readings and steady state error of the calorimeter is determined using a controllable pseudo battery. The pseudo battery is made using a silicone heating pad (Omega Inc SRFR-609) with the same dimensions as the battery. The heat generation rate of the pseudo battery is controlled via a variable voltage supply (Keithley 2700). Calibration tests are performed with a heater output of 10 W for 2 h, during which the response of the system reaches steady state. After 2 h, the heater is turned off, creating a step down in heat generation rate. The calorimeter is allowed to return to the initial conditions, and the calibration process is repeated for all the operating temperatures of the battery tests.

The standard deviation of the temperature measurements over 1000 s after the calorimeter reached steady state is calculated for ten separate tests, with the same heat generation rate and operating temperatures. The standard deviation values of the ten tests are averaged and calculated to be 0.025 °C. Smoothing parameter p can be tuned using the obtained value of measurement error. Beck's method is applied to the temperature measurements with various values of p in order to calculate the heat flux at the surface of interest. The calculated heat flux is then used in Equation (4) to calculate the projected temperature at a distance of 4 mm away from the surface of interest (same location as the thermocouple). Parameter p is adjusted such that the RMS error of the projected temperature matched the standard deviation of the actual temperature measurement, with the final, adjusted value of p being 100.

Beck's method (with $p = 100$) is applied to the measured temperature data to calculate the applied heat flux at the surface of interest for all operating temperatures tested. A comparison between the calculated heat generation rate using Beck's method and the actual heat generation rate of the heater at an operating temperature of 10 °C is shown in Fig. 5. The difference in the surface temperatures of the pseudo battery at the beginning of validation test and the step down event in heat generation signifies that there is stored heat in the pseudo battery. The calculated heat generation rate using Beck's Method is capable of detecting the step down event in the heat output of the pseudo battery despite of the stored heat. The calibration process is repeated for all the operating conditions of the calorimeter with the same heat input, the results of which are shown in Table 1. It is seen that accuracy is between 80% and 85%, and on average, the heat lost to the environment which the calorimeter cannot account for is approximately 2 W.

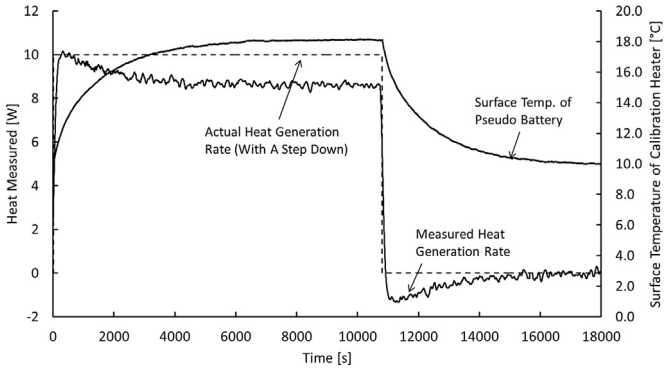

Fig. 5. Comparison of the measured heat generation rate using Beck's Method (solid line) and the actual heat output from calibration heater (dashed line) at 10 °C for a step down in heat output. Surface temperature refers to the temperature measured at the contact surface between the pseudo battery and the high density polyethylene (HDPE) slab.

Table 1
Accuracy and standard deviation of heat generation measured by battery calorimeter for varying operating temperatures.

Operating temp.	[°C]	40	30	20	10	0	−10
Accuracy	[%]	81	84.4	83.8	84.1	82.0	80.1
Standard deviation	[W]	0.061	0.052	0.020	0.041	0.017	0.066

3. Results and discussion

The $LiFePO_4$ battery is tested as described in Section 2. All results shown in this section are average measurements of five repetitive tests. The maximum standard deviation in battery voltage throughout discharge for all tested operating temperatures is 0.13 V for 3C discharge, while the open circuit voltage of the test battery is 3.6 V. The rate of heat generation is dependent on two main parameters: discharge current and battery temperature. The following sections will summarize the observed effects of both battery discharge rate and operating temperature on battery heat generation rates.

3.1. Effect of battery discharge rate on heat generation rate

Fig. 6 shows the measured heat generation rates of the battery for all tested discharge rates at 20 °C as a function of depth of discharge (varying from 0 to 1). There is a clear increase in battery heat generation throughout discharge at increased rates of discharge due to the higher irreversible heat generation. Irreversible heat generation is a function of current squared, whereas reversible heat generation is a linear function of current [9]; therefore increasing the discharge current causes a corresponding change in the proportion of the irreversible heat generation in the total heat generation of the battery. The total battery heat generation at 0.25C is shown to be almost negligible when compared to the total amount of heat generated when the battery is discharged at 3C at 20 °C.

The heat generation can be non-dimensionalized by dividing the heat generated during battery discharge by the instantaneous amount of electrical power drawn from the battery. Non-dimensionalized heat generation provides a clearer representation of the heat generation characteristics throughout the discharge test, as shown in Fig. 7. It can be seen that the proportion of heat

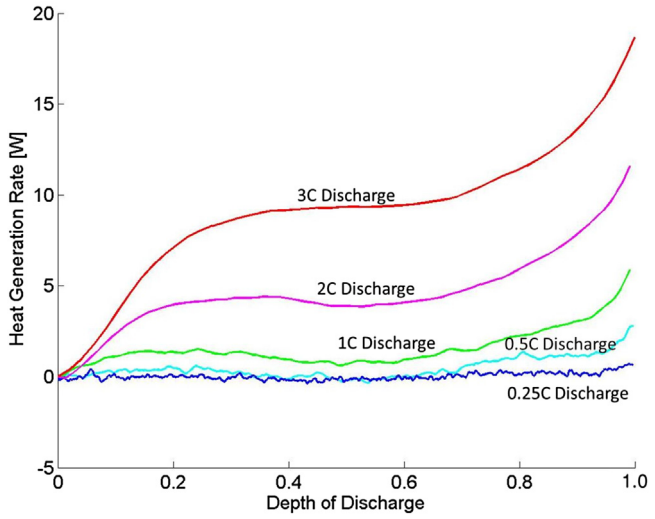

Fig. 6. Effect of tested discharge rates on the heat generation rate of an A123 $LiFePO_4$ battery at an operating temperature of 20 °C.

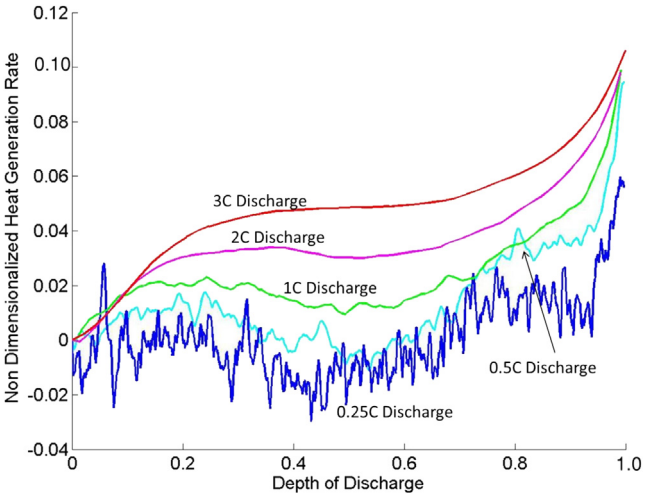

Fig. 7. Effect of discharge rate on the heat generation rate, non-dimensionalized by electrical power drawn, of A123 $LiFePO_4$ battery at an operating temperature of 20 °C.

generated to the instantaneous power drawn from the battery is under 0.10 for all discharge rates, regardless of discharge current. This shows that the proportion of electrical energy lost due to conversion to waste heat is on the same order of magnitude for all discharge rates.

The increase in non-dimensionalized heat generation at the higher rates of discharge can be related to two main factors: increased Joule heating at the battery current collectors and increased battery overpotentials at higher rates of discharge. Increases in battery discharge current directly increases the amplitude of the Joule heating due to increased current density near the current collectors. The overpotentials of the battery increase as the current drawn from the battery is increased according to the Tafel equation [3]. There is an increased amount of noise in the determined heat generation value for discharge rates less than 1C, caused by increased noise to signal ratio at lower battery heat generation rates.

As the discharge rate of the battery is decreased to less than 1C, irreversible heat generation (which is always exothermic) is reduced, and endothermic heat flow due to reversible heat generation can be observed in the measured heat generation curves. Fig. 8 shows the heat generation profile at 0.5C discharge rate with the corresponding voltage discharge curves. Endothermic heat flow for 0.5C discharge rate can be observed for the battery operating temperatures of 30 °C and 40 °C. At a 0.25C discharge rate, endothermic heat flow during discharge can be observed for the battery operating temperatures from 0 °C to 40 °C [26]. Due to equipment limitations, endothermic reactions could not be calibrated using the experimental setup.

Non-uniform current distribution and concentration gradients on the electrodes due to limits in mass transfer can cause heat of mixing, which could be endothermic during the discharge [27]. The development of current and concentration gradients in the battery is caused by high discharge rates required of Li-ion batteries due to sudden EV acceleration. The amount of heat absorbed during the formation of the gradients will be released after the end of battery discharge, as the developed gradients relax to equilibrium. Heat of mixing increases at higher rates of discharge, and has been cited as a significant contributor to battery heat generation at discharge rates higher than 1C [17,27].

As the battery discharge stops, the heat generated by the battery should theoretically go to 0. Therefore, the existence of heat of mixing can be confirmed by examining the heat generation

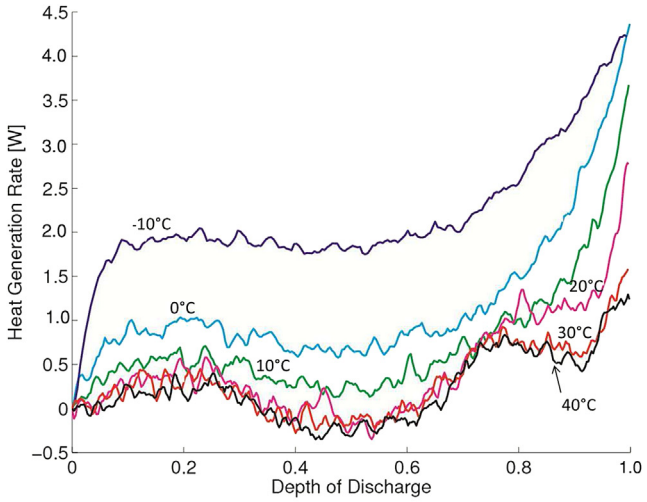

(a) Heat generation

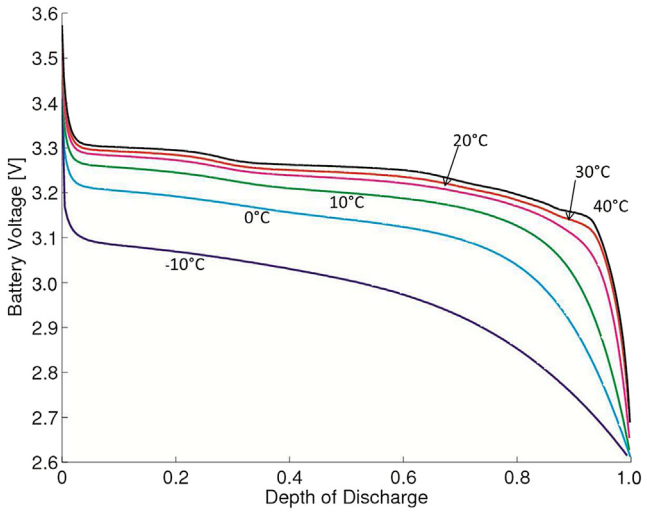

(b) Battery discharge curve

Fig. 8. Effect of battery operating temperature on (a) heat generation rate and (b) battery discharge curve for an A123 $LiFePO_4$ battery at 0.5C discharge.

characteristics of the battery after the end of discharge. Fig. 9 shows the existence of heat generation after battery discharge terminates at 1C and 20 °C where the heat generated by the battery after the end of discharge is representative of 16% of the total heat generation. It is shown in Section 2.4 that the data reduction technique is capable of detecting a step down in heat generation rate despite heat stored in the calibration test apparatus, therefore it is unlikely the observed heat generation phenomenon is due to the stored heat in the system.

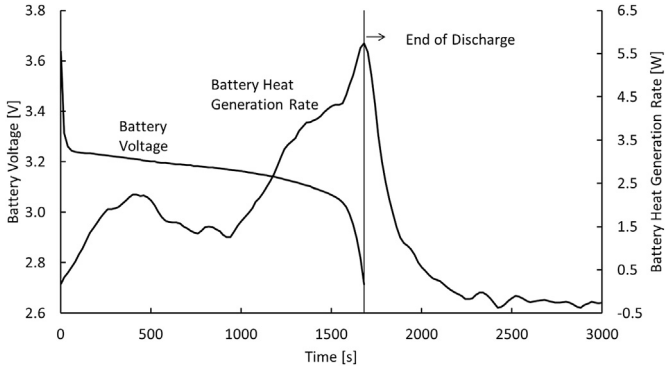

Fig. 9. Battery discharge curve and measured heat generation profile of an A123 $LiFePO_4$ battery, for 1C discharge at 20 °C. Measurements show the presence of additional heat generation post end of discharge.

Heat of mixing has been observed for small cylindrical Li-ion batteries, though only for discharge rates higher than or equal to 1C [16,17]. The contribution of heat of mixing to the total heat generation of small cylindrical Li-ion batteries is generally neglected for discharge rates lower than 1C [21,28]. For this study, the heat of mixing can be observed for the lowest discharge rate tested (0.25C), at both 40 °C and −10 °C, as seen in Fig. 10a and b respectively. Heat generation after the end of discharge contributes significantly to the total heat generated by the battery, accounting for 13% of the total heat generation at −10 °C. Therefore, heat of mixing for large prismatic Li-ion batteries should not be ignored at discharge rates higher than 0.25C.

3.2. Effect of operating temperature on heat generation rate

Fig. 11a shows the battery heat generation rate profiles at various battery operating temperatures for a 1C discharge rate. It is seen that heat generation rates are greatly increased at lower temperatures, signifying the degradation of battery performance substantially.

Battery internal resistance, the main cause of the irreversible heating, is dependent on the temperature. Previous work on small, cylindrical Li-ion batteries has shown a strong dependence of

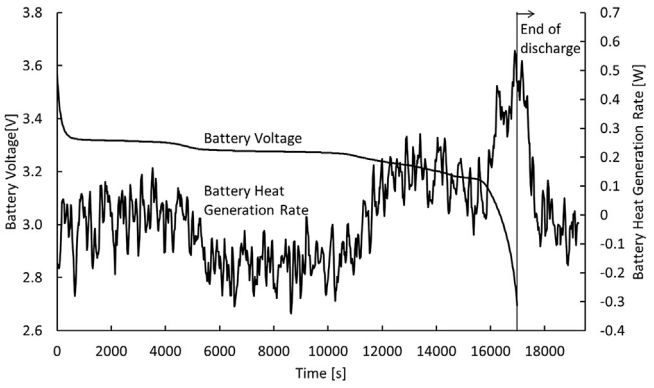

(a) 40°C

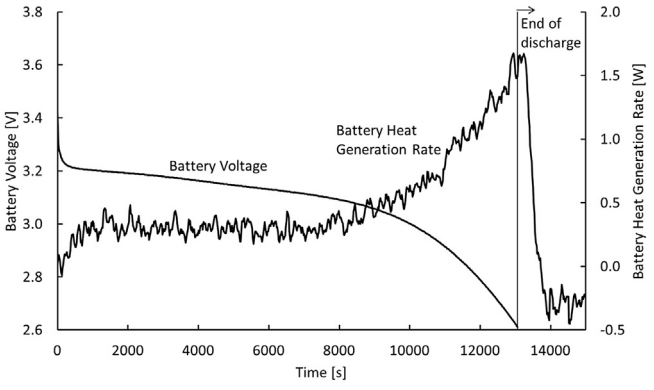

(b) -10°C

Fig. 10. Battery discharge curve and measured heat generation profile of an A123 $LiFePO_4$ battery, at 0.25C discharge, showing battery heat generation post the end of discharge for operating temperatures of (a) 40 °C, and (b) −10 °C.

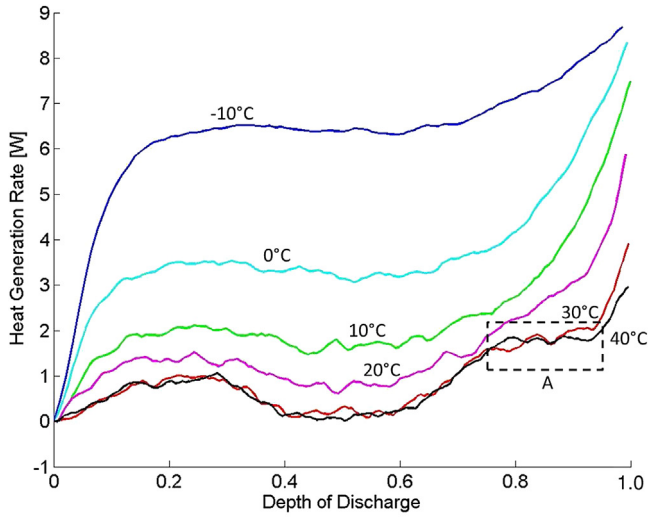

(a) Heat generation

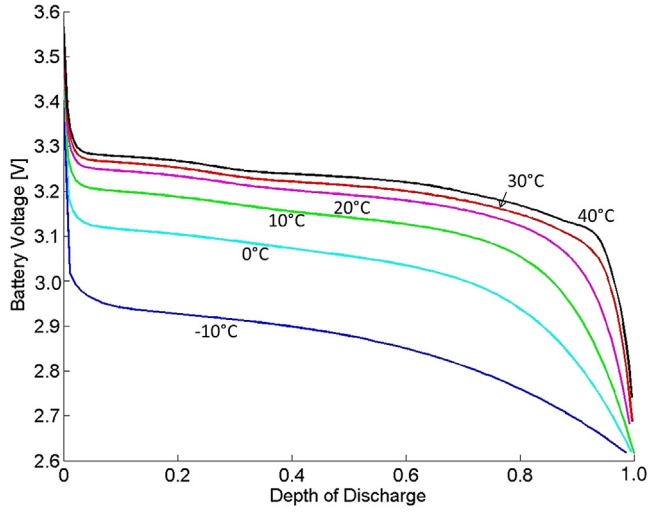

(b) Battery discharge curve

Fig. 11. Effect of battery operating temperature on (a) the heat generation rate and (b) the battery discharge curve of an A123 $LiFePO_4$ battery, for 1C discharge.

battery internal resistance on temperature, and the increase in battery internal resistance at low temperatures causes an increased amount of irreversible heat generation [29–31]. Decreased battery heat generation at higher operating temperatures is also due to increased rates of mass transport and reduced activation loss which decreases overpotential during discharge. Decreased overpotential translates to the diminished rates of irreversible heat generation at the beginning of discharge. The heat generation rates of the battery at 30 °C and 40 °C is very similar at a 1C discharge rate despite the decreased irreversible heat generation rate. This shows that the proportion of reversible heat generation increases as battery operating temperature increases.

Battery discharge curves corresponding to the heat generation profiles at 1C discharge for all tested operating temperatures can be seen in Fig. 11b. Discharge from −10 °C to 20 °C shows quasi-linear voltage drops with respect to depth of discharge, similar to what is commonly seen in literature. At battery operating temperatures higher than 20 °C, two low frequency fluctuations in battery discharge curve are visible, the first of which occurs at a DOD of approximately 0.3, and the second at a DOD of approximately 0.8. This phenomenon has not been seen in literature for $LiFePO_4$ battery; it is commonly seen in Li-ion batteries of $LiMnO_4$ chemistry, and is caused by phase change mechanisms during discharge [18,21].

As the amount of irreversible heat decreases at higher battery operating temperatures, additional features in the heat generation profile is more visible. Fig. 11a shows a distinct decrease in heat generation at a depth of discharge (DOD) of approximately 0.3, with heat generation reaching a minimum at a DOD of approximately 0.5 for all battery operating temperatures. At battery temperatures of 0 °C, 10 °C, and 20 °C, the decreased rate of heat generation causes the overall measured heat generation profile to form a distinct S-shape, with a single peak in exothermic heat flow during discharge. For operating temperatures higher than 20 °C, a plateauing of heat generation is observed at a DOD of approximately 0.8 (shown as area A in Fig. 11a). A comparison of the heat generation profiles of the battery at 0 °C and 40 °C is shown in Fig. 12. The secondary plateau in heat generation rate can be observed for all discharge rates tested at 40 °C, as shown in Fig. 12a, but is not visible for

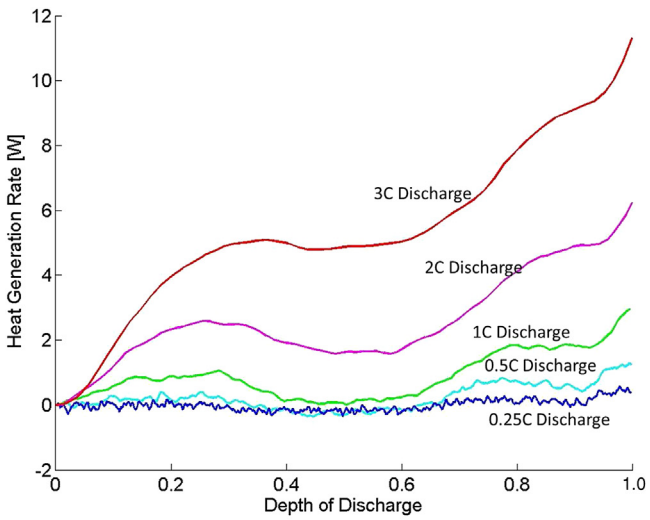

(a) 40°C

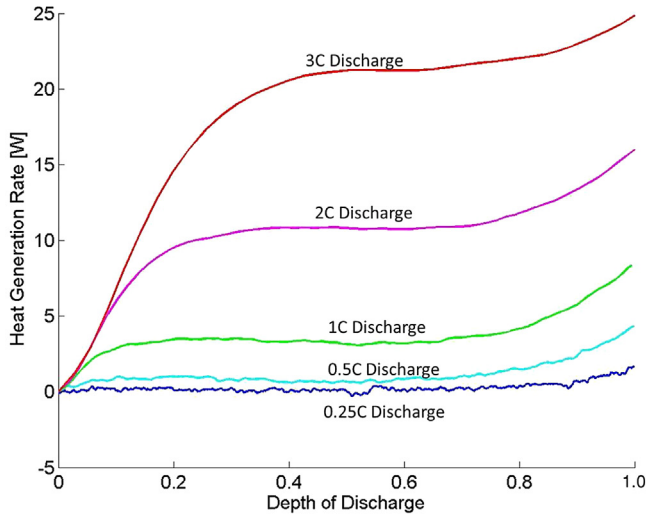

(b) 0°C

Fig. 12. Heat generation rate of an A123 $LiFePO_4$ battery at (a) 40 °C and (b) 0 °C for all tested discharge rates. Secondary plateauing in heat generation rate at a depth of discharge of 0.8 can be observed for all discharge rates tested at 40 °C.

battery operating temperature of 0 °C (Fig. 12b). This shows the dependence of the observed secondary plateauing phenomenon on the operating temperature of the battery.

The observed features in the heat generation profile of the battery is more discernible at high battery operating temperatures. The transitions between plateaus in the battery discharge curve correspond to rapid change in the measured heat generation rates of the battery for 0.25C discharge at 30 °C and 40 °C, as seen in Fig. 13.

The decrease in heat generation during discharge can be attributed to phase change mechanisms, which corresponds to transition regions between voltage plateaus in the battery discharge curves of $LiMnO_4$ batteries [20,32]. Phase change mechanisms in $LiFePO_4$ remain a topic of investigation, with the existence of multiple models that are supported by experimental data [33]. Most models show the existence of only two phases in the phase change process [34,35], although recent developments have shown the existence of transient phase changes through *in-situ* observations [36]. Double plateaus in voltage curve has been attributed to a double phase change in $LiMnO_4$ batteries [18,21] which leads to the hypothesis that the presence of a double phase change is possible for $LiFePO_4$ batteries at higher battery operating temperatures at low discharge rates. The double plateau in the battery voltage for $LiFePO_4$ at higher battery operating temperatures have not been reported in literature.

Through observations of heat generation phenomena in the tested $LiFePO_4$ battery, commonly used heat generation equations [9] need to be modified to accurately model the complex heat generation characteristics of $LiFePO_4$ batteries. The fluctuations in heat generation rate and the double plateauing of the battery discharge curve at increased operating temperatures and decreased discharge rates warrants further investigation for better understanding of the phase change and heat generation mechanisms of large prismatic Li-ion batteries.

3.3. Validation of results

The calculated heat generation rates of the battery using Beck's Method can be validated using the same experimental validation setup as discussed in Section 2.4. The pseudo battery comprising of the flexible silicone heater between two steel sheets takes the place of the actual battery inside the calorimeter, and its heat output is that of the measured heat generation rate of the actual battery. The temperature change within the HDPE slabs due to the heat

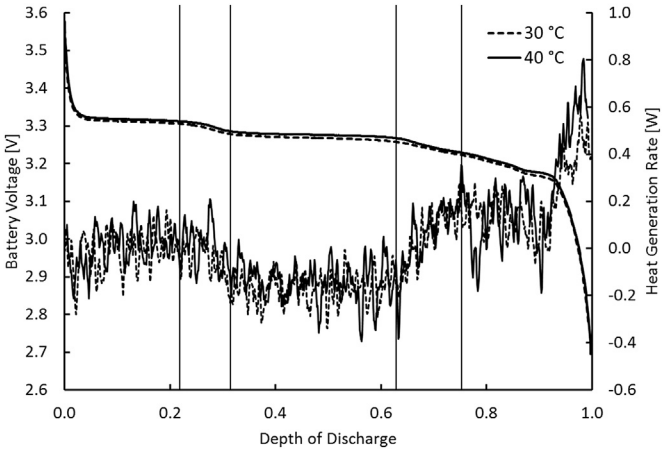

Fig. 13. Heat generation rates and battery discharge curves for 0.25C discharge at 30 °C and 40 °C. Transitions between voltage discharge curve plateaus correspond to regions of rapid change in the measured battery heat generation.

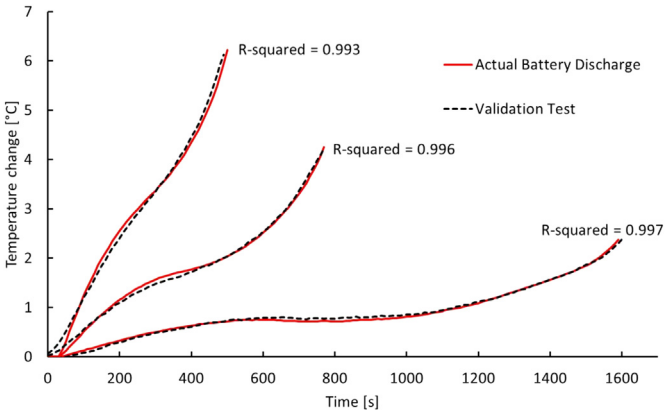

Fig. 14. Comparison of the temperature measurements for the validation test and actual battery discharge for 1C, 2C and 3C discharge rates at an operating temperature of 20 °C.

generated by both the pseudo and test batteries are compared. A high coefficient of determination between the two system responses denotes that the measured heat generation rates of the test battery is accurate.

The measured heat generation rates of the test battery at 1C, 2C, and 3C discharge are used as heat output of the pseudo battery. Heat flow from the battery at discharge rates of 0.25C and 0.5C at high battery operating temperatures can be endothermic, which cannot be recreated by the pseudo battery and hence will be excluded from the validation tests. A comparison of the temperature increase between the validation and actual battery discharge tests at the temperature of 20 °C is shown in Fig. 14. At 20 °C, the measured temperature increase within the HDPE slab for both the validation and battery discharge test is very close, achieving an R-squared value of above 0.99 for all discharge rates validated.

For other battery operating temperatures and discharge rates, the average temperature increase within the HDPE slab for the validation test and actual battery discharge achieve a minimum R-squared value of 0.98. The largest variations between the measured response of the calorimeter during real battery testing and pseudo battery testing occurs at high temperatures when the heat flow from the battery reaches near endothermic levels. This shows that the obtained results using Beck's method is a good representation of the actual heat generation rates of the battery for all operating temperatures and discharge rates investigated.

A summary of the measured total heat generation rates at the tested discharge rates and temperatures is shown in Table 2. The results are shown as a range due to the variation of heat generation rate of the battery throughout discharge. It can be seen that the minimum measured heat flow from the battery are endothermic at 0.25C discharge, for the majority of tested temperatures. Complete heat generation curves throughout discharge for all tested discharge rates and battery operating temperatures are available elsewhere [26].

Table 2
Summary of measured $LiFePO_4$ heat generation rates at all tested discharge rates and battery operating temperatures.

Temp. [°C]	Discharge rate				
	0.25C	0.5C	1C	2C	3C
−10	0 to 2.09	0 to 5.29	0 to 10.82	0 to 24.71	–
0	−0.33 to 2.05	0 to 5.20	0 to 10.21	0 to 19.52	0 to 29.93
10	−0.24 to 1.43	0 to 4.37	0 to 8.87	0 to 16.72	0 to 24.79
20	−0.44 to 0.87	0 to 3.32	0 to 4.92	0 to 13.78	0 to 4.92
30	−0.46 to 0.85	−0.33 to 1.86	0 to 4.56	0 to 10.39	0 to 16.48
40	−0.43 to 0.71	−0.44 to 1.62	0 to 3.70	0 to 7.88	0 to 14.21

4. Conclusion

In this work, a method of heat generation measurement for a prismatic battery is presented, which is applicable to any prismatic battery regardless of chemistries. The heat generation rate of a 20 Ah prismatic A123 $LiFePO_4$ battery is measured under a wide range of discharge rates and operating temperatures. It is shown that the heat generation rate of the tested battery increases with the discharge rate, and decreases with the operating temperature. Heat of mixing is observed at a discharge rate as low as 0.25C for all tested battery operating temperatures. The magnitude of the heat of mixing at −10 °C for 0.25C discharge accounts for 13% of the overall heat generated during discharge and hence cannot be ignored for prismatic $LiFePO_4$ batteries. Measured heat generation rates follow an S-shape profile, with exothermic heat flow at the beginning and end of discharge, and a decrease in heat generation rate at a depth of discharge of approximately 0.3. For rates of discharge lower than 1C, the decrease in heat flow is reduced to endothermic levels, especially at high battery operating temperatures. A visible secondary plateau in heat generation can be observed for increased battery operating temperatures at a depth of discharge of approximately 0.8. Transitions between the voltage discharge curve plateaus correspond to regions of rapid change in measured battery heat generation. Double plateaus in battery discharge curve show the possibility of a double phase change mechanism at lower rates of discharge for high battery operating temperatures.

Acknowledgement

The financial support for this study is provided by the Ontario Research Fund-Research Excellence (ORF-RE) program via contract number # RE-02-019 and the Natural Sciences and Engineering Research Council of Canada (NSERC) via the Discovery Grant.

References

[1] T.M. Bandhauer, S. Garimella, T.F. Fuller, J. Electrochem. Soc. 158 (2011) R1–R25.
[2] L. Cheng, C. Ke, S. Fengchun, in: IEEE Vehicle Power Propulsion Conference, 2009, pp. 1643–1648.
[3] T. Reddy, Linden's Handbook of Batteries, McGraw-Hill Inc., 2011.
[4] K. Vetter, P. Novak, M. Wagner, C. Veit, K. Moller, J.O. B, M. Winter, M. Wohlfahrt-Mehrens, C. Vogler, A. Hammouche, J. Power Sources 147 (2005) 269–281.
[5] S. Santhanagopalan, Q. Zhang, K. Kumaresan, R. White, J. Electrochem. Soc. 155 (2008) A345–A353.
[6] S. Zhang, K. Xu, T. Jow, J. Power Sources 115 (2003) 137–140.
[7] C. Pals, J. Newman, J. Electrochem. Soc. 142 (1995) 3274–3281.
[8] G. Botte, B. Johnson, R. White, J. Electrochem. Soc. 146 (1999) 914–923.
[9] D. Bernardi, E. Pawlikowski, J. Newman, J. Electrochem. Soc. 132 (1985) 5–12.
[10] W. Gu, C. Wang, J. Electrochem. Soc. 147 (2000) 2910–2922.
[11] U. Kim, C. Shin, C. Kim, J. Power Sources 180 (2008) 909–916.
[12] U. Kim, C. Shin, C. Kim, J. Power Sources 189 (2009) 841–846.
[13] W. Wu, X. Xiao, X. Huang, Electrochim. Acta 83 (2012) 227–240.
[15] G. Kim, A. Pesaran, R. Spotnitz, J. Power Sources 170 (2007) 476–489.
[16] J. Hong, H. Maleki, S. Al Hallaj, L. Redey, J. Selman, J. Electrochem. Soc. 145 (1998) 1489–1591.
[17] S. Al Hallaj, J. Prakash, J. Selman, J. Power Sources 87 (2000) 186–194.
[18] J. Kim, J. Prakash, J. Selman, Electrochem. Solid-State Lett. 4 (2001) A141–A144.
[19] Y. Kobayashi, H. Miyashiro, K. Kumao, T. Takei, K. Iwahori, I. Uchida, J. Electrochem. Soc. 149 (2002) A978–A982.
[20] K. Onda, H. Kameyama, H. T, K. Ito, J. Electrochem. Soc. 150 (2003).
[21] H. Bang, H. Yang, Y. Sun, J. Prakash, J. Electrochem. Soc. 152 (2005) A421–A428.
[22] W. Hemminger, G. Hoehne, Calorimetry, Fundamentals and Practice, Verlag Chemie, 1984.
[23] J. Beck, B. Blackwell, C. St-Clair, Inverse Heat Conduction, Ill Posed Problems, John Wiley and Sons, Inc., 1985.
[24] J. Beck, B. Blackwell, A. Haji-Sheikh, Int. J. Heat Mass Transfer 39 (1996) 3649–3657.
[25] K. Woodbury, S. Thackur, Inverse Probl. Eng. 2 (1996) 319–333.
[26] K. Chen, Calorimetric Heat Generation Measurements of Prismatic Lithium Ion Batteries (Master's thesis), University of Waterloo, 2013.
[27] K. Thomas, J. Newman, J. Power Sources 119 (2003) 844–849.
[28] W. Lu, H. Yang, J. Prakash, Electrochim. Acta 51 (2006) 1322–1329.
[29] Y. Inui, Y. Kobayashi, Y. Watanabe, Y. Watase, Energy Convers. Manage. 48 (2007) 2103–2109.
[30] H. Kameyama, T. Hanamoto, K. Ito, Y. Inui, K. Onda, IEEE Trans. Energy Convers. 112 (2002) 1192–1199.
[31] J. Kim, S. Lee, J. Lee, B. Cho, in: IEEE International Conference on Power Electronics, 2007, pp. 1173–1178.
[32] S. Al Hallaj, R. Venjatachalapath, J. Prakash, J.R. S, J. Electrochem. Soc. 147 (2000) 2432–2436.
[33] C.T. Love, A. Korovina, C. Patridge, K. Swider-Lyones, M. Twigg, D. Ramaker, J. Electrochem. Soc. 160 (2013) A3151–A3161.
[34] V. Srinivasan, J. Newman, J. Electrochem. Soc. 151 (2004) A1517–A1529.
[35] A. Yamada, H. Koizumi, N. Sonoyama, R. Kanno, Electrochem. Solid State Lett. 8 (2005) A409–A413.
[36] Y. Orikasa, T. Maeda, Y. Koyama, H. Murayama, K. Fukuda, H. Tanida, E. Arai, H. amd, Matsubara, Y. Uchinoto, Z. Ogumi, Chem. Mater. 25 (2013) 1032–1039.